

NUMERICAL MODELLING OF MASONRY-LIKE MATERIALS UNDER CYCLIC LOADING

HÉLOÏSE ROSTAGNI*, CÉDRIC GIRY* AND FRÉDÉRIC RAGUENEAU*†

*Université Paris-Saclay, CentraleSupélec, ENS Paris-Saclay, CNRS,
Laboratoire de Mécanique Paris-Saclay (LMPS)
Gif-sur-Yvette, France
e-mail: heloise.rostagni;cedric.giry;frederic.ragueneau@ens-paris-saclay.fr

†EPF École d'Ingénieurs
Cachan, France

Key words: Masonry, Quasi-brittle, Damage, Non-local, Dissipation

Abstract. This paper presents a constitutive model to describe the non-linear mechanical response of masonry. This heterogeneous material is represented by a fictitious homogeneous medium whose natural basis is defined by the material texture, *i.e.* its joint planes. The model takes into account the elastic orthotropy of the material as well as the main degradation mechanisms: damage and friction. This thermodynamics-based model is used to estimate the dissipations. This model is implemented in a finite element code and validated at the Gauss point scale. It is then used to evaluate the response of structures subjected to monotonic and cyclic multi-directional loading. An analysis of regularisation methods (energetic and non-local integral) is proposed. This model provides a reliable representation of the overall behaviour of masonry, with the possibility of studying dissipative mechanisms independently.

1 INTRODUCTION

Masonry structures represent a large part of the existing architectural and cultural heritage. When exposed to natural or anthropic hazards, these structures may experience significant structural damage, resulting in their collapses. Developing efficient and accurate tools to represent their degradation and assess their vulnerability is crucial to maintain their structural integrity. Recent seismic events have highlighted this need. Examples include the earthquakes in L'Aquila (Italy, 2009) and Amatrice (Italy, 2016), which largely destroyed these towns, and the earthquake in Le Teil (France, 2019), which caused major damage to historical structures (Castle of Saint-Tomé, Church of Saint-Étienne de Melas).

This work focuses on masonry with orthogonal joints (see Fig. 1). Several models have been developed or adapted for masonry over the previous decades (*e.g.* [12] [18], [11], [20], [1], [19], [23]). Macroscopic finite element models are the most widely used to describe large structures, but some of them have difficulties in representing the non-linear anisotropic nature of the material.



Figure 1: Regular bonded masonry.

A thermodynamically based friction-damage model for masonry is developed in this work.

The mechanical behaviour of masonry exhibits a softening phase typical of quasi-brittle materials. Local continuum damage models fail to represent the entire degradation process: the decrease in stress (with increasing strain) leads to a peak around which bifurcations towards localised solutions appear. Knowing which solutions reflect the failure process is impossible; the strain localisation phenomenon caused by softening cannot be captured objectively. From a numerical point of view, finite element calculations suffer from mesh dependency. Physical inconsistencies can be observed in the numerical results: the process zone size is directly related to the mesh one, implying that the energy dissipated at failure tends towards zero as the mesh is refined. To overcome this problem, a characteristic length representative of the interactions at the microstructure scale of the material is introduced into the solution. Different regularisation methods have been developed in the literature to limit the localisation of deformations and degradations in softening media and to recover objectivity (*e.g.* [7], [16], [17]).

In this model, an energy regularisation approach is first tested which explicitly relates the intrinsic dissipation energy of the material to the size of the finite elements. Then, an integral non-local regularisation is used by introducing non-locality on an internal variable linked to the evolution of the damage through a characteristic length generating a circular averaging zone. This model and the regularisation methods were implemented in finite element software and tested at the structure's scale on a panel.

2 MASONRY MODELLING

Masonry is described as a homogeneous material whose main orthotropic base (1, 2, 3) is related to its orthogonal joint planes (Fig. 2). In this material, damage evolution is mainly governed by mortar joints leading to orthogonal crack patterns (Fig. 3). The model based on Continuum Damage Mechanics proposes an orthotropic degradation description through the decomposition of crack families along the nat-

ural directions of masonry joints. An additional damage variable is also introduced to represent the crushing of blocs during compression loading. The unilateral effect (recovery of stiffness during crack reclosure) and the internal sliding (hysteretic dissipation and permanent deformations generated due to friction at the crack surface) are introduced to reproduce its behaviour under cyclic loading. The Gibbs energy of such a model gives rise to the formulation of an intrinsic dissipative energy that allows degradation mechanisms to be taken into account. The complete model is given in [21]. Only the equations related to damage, regularisation and dissipation are recalled.

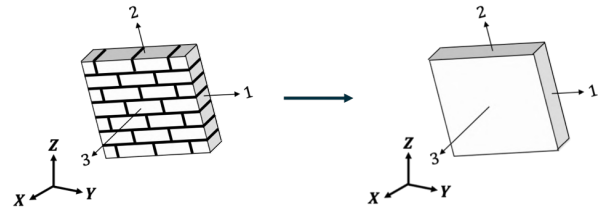


Figure 2: (left) Explicit and (right) homogenised descriptions of masonry.

2.1 Damage

When subjected to mechanical stress, masonry will degrade and dissipate energy. In most cases, this will lead to the formation of cracks that will follow the joint planes (Fig. 3). The development of damage in the material is modelled by the decomposition of the compliance tensor representing the impact of a network of orthogonal and independent cracks along the joint planes (Fig. 4). The damage then affects the elastic moduli by means of an effect tensor $\mathbb{A}^{(i)}$ whose expression is inspired by models for composite materials [13] and a scalar variable d_i [9], varying from 0 for the absence of cracks in the i direction to $+\infty$ for a fully degraded material in this direction (Eq. (3)). Effective compliance can be calculated by:

$$\mathbb{S}^{eff} = \mathbb{S}^0 + \Delta\mathbb{S}0 = \mathbb{S}^0 + \sum_{i=1}^3 d_i (\mathbb{A}^{(i)} : \mathbb{S}^0) \quad (1)$$

Local evolution: the evolution of cracking is

governed by both the extension of the material and the shear deformations through an equivalent strain $\tilde{\varepsilon}_i$:

$$\tilde{\varepsilon}_i = \sqrt{\langle \varepsilon_i \rangle_+^2 + \beta_{il} \varepsilon_{il}^2 + \varepsilon_{im}^2},$$

with $(i, l, m) = (1, 2, 3)$, (2)

where β_{il} and β_{im} are material coefficients modulating the impact of shear deformations on the yield strength and damage evolution. It is directly involved in the damage threshold function which, by applying the load-unload conditions, gives the evolution law (Eq. (3)) with k_i the equivalent strain threshold which initiates damage in the i direction and χ_i a brittleness parameter.

$$d_i = \frac{\tilde{\varepsilon}_i}{k_i} \exp[\chi_i (\tilde{\varepsilon}_i - k_i)] - 1,$$

with $i \in \llbracket 1; 3 \rrbracket$. (3)



Figure 3: Examples of cracks in bonded masonry structures [5].

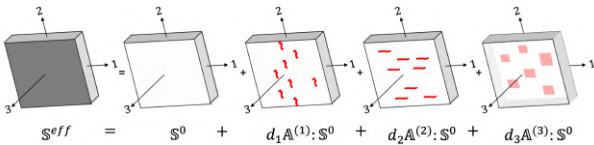


Figure 4: Effect of crack families on the compliance tensor [21].

2.2 Regularisation

Regularisation techniques must be adopted to limit the mesh dependency of the solution obtained using the finite element method. Various methods have been developed in the literature to maintain the objectivity of the results with respect to the mesh when locating deformations (e.g. [6], [17], [16], [2], [14], [15], [4]). In this work, the following two methods are used:

Fracture energy regularisation [7]: an explicit relationship between the intrinsic dissipated energy of the material and the size of the elements is introduced in order to ensure energy dissipation independent of mesh refinement. The parameters of the damage evolution law are adjusted to dissipate the amount of energy G_{fi} in each finite element. For each element, a characteristic size h_i of the element along the normal direction of the crack is taken into account, and the fracture energy is then written according to the equation (4).

$$G_{fi} = \int_0^\infty \sigma_i d\varepsilon_i$$

$$\rightarrow \chi_i = \frac{E_i h_i k_i}{G_{fi} - 0.5 h_i E_i k_i^2}$$

with $i \in \llbracket 1; 3 \rrbracket$. (4)

However, this method does not eliminate all biases, as it is dependent on the orientation of the elements [8].

Non-local integral regularisation [17]: the non-local nature of the degradation process is taken into account. Local equivalent strains are replaced by their associated non-local counterpart, taking into account the influence of the neighbourhood. In this way, damage in each of the i directions is controlled by the non-local variable $\bar{\varepsilon}_i$:

$$\bar{\varepsilon}_i = \frac{\int_\Omega \alpha(x, s, l_c) \tilde{\varepsilon}_i(s) ds}{\int_\Omega \alpha(x, s, l_c) ds}$$

with $i \in \llbracket 1; 3 \rrbracket$. (5)

where $\alpha(x, s, l_c)$ is a weight function depending on the distance between a source point s and a target point x and an internal length l_c .

It is classically taken as a Gaussian distribution. These non-local variables are then directly involved in the expression of the damage d_i (Eq. (3)) in which $\tilde{\varepsilon}_i$ is replaced by $\bar{\varepsilon}_i$.

2.3 Dissipation

The total intrinsic dissipation \mathcal{D} is deduced from the thermodynamic potential Ψ through the Clausius-Duhem inequality (Eq. (6)) [10].

$$\dot{\mathcal{D}} = \sigma \cdot \dot{\varepsilon} - \rho \dot{\Psi} \geq 0. \quad (6)$$

\mathcal{D} can be decomposed into two terms (Eq. (7)) related to the main degradation mechanisms (damage, internal sliding and friction).

$$\begin{aligned} \dot{\mathcal{D}} &= \dot{\mathcal{D}}_{damage} + \dot{\mathcal{D}}_{sliding} \\ &= \left[Y_i \dot{d}_j \right] + \left[\sigma_k^\pi \dot{\varepsilon}_k^\pi - X_k \dot{\alpha}_k^\pi \right] \\ &\quad \text{with } (i, k) \in \llbracket 1; 3 \rrbracket \times \llbracket 4; 6 \rrbracket. \end{aligned} \quad (7)$$

Y_i , ε_k^π , σ_k^π , X_k and α_k represent respectively the energy restitution rates, the anelastic frictional strains and stresses, the kinematic strain hardening variables and those thermodynamically associated.

The energy dissipated is estimated graphically from the experimental curve $E_d^{(1)}$ (Eq. (8)) and calculated from the numerical results $E_d^{(2)}$ (Eq. (9)).

$$E_d^{(1)} = \int_{\varepsilon_j} \sigma_j d\varepsilon_j \quad (8)$$

$$E_d^{(2)} = \frac{1}{\mathcal{V}} \int_{\mathcal{V}} \int_{\tau} \dot{\mathcal{D}} dt d\Omega \quad (9)$$

These names, $E_d^{(1)}$ and $E_d^{(2)}$, will be referred to in the following section.

3 RESULTS

3.1 Gauss point validation

The model was implemented in the MFront software [<http://tfel.sourceforge.net>] and tested on a hardware point using the MTest module. Three tests were carried out in order to highlight the main dissipative mechanisms of the model.

Unidirectional tension-compression test: this test illustrates the evolution of damage and the unilateral effect (Fig. 5). A strain loading is applied: ε_{22} varies from 0 to $3.5 \cdot 10^{-4}$, then decreases to $-1.2 \cdot 10^{-4}$ and increases up to $5.5 \cdot 10^{-4}$. It decreases again to $-2 \cdot 10^{-4}$ before increasing again to $8 \cdot 10^{-4}$ (Fig. 5a). When the damage threshold is exceeded, a softening phase is observed (Fig. 5b). The unloading phase shows the degradation of the elastic modulus and is followed by a recovery of stiffness when the stress becomes negative (compression). The evolution of D_2 as a function of strain in the loading direction (Fig. 5c) shows that damage remains zero until k_2 is exceeded, then it increases progressively with strain. During discharge, D_2 remains constant (no compression damage D_c). Only damage in the direction of the load is activated.

Cyclic shear test without pre-compression: this test activates the coupling between the damage and friction mechanisms (Fig. 6). The following load is applied: ε_{12} varies from 0 to $7.5 \cdot 10^{-4}$, then decreases to $-2.5 \cdot 10^{-4}$ and increases up to $3.0 \cdot 10^{-3}$ (Fig. 6a). The shear modulus degrades as the material becomes damaged (Fig 6b). The presence of a hysteresis loop during the unloading-reloading phase indicates the development of friction at the crack interface. A mismatch between the two shear-activated damages is observed due to the orthotropic behaviour of the masonry (Fig. 6c).

Cyclic shear test with a pre-compression of 0.2MPa: this test shows the response of the model under non-proportional loading and highlights the influence of confinement (Fig. 7). The lateral loading is the same as in the previous test. A response similar to the case without pre-compression is obtained; however, the width of the hysteresis loop increases with confinement (Fig 7b). For the damage variables (Fig. 7c), similar evolutions are observed with and without confinement, the latter mainly impacting the friction mechanism.

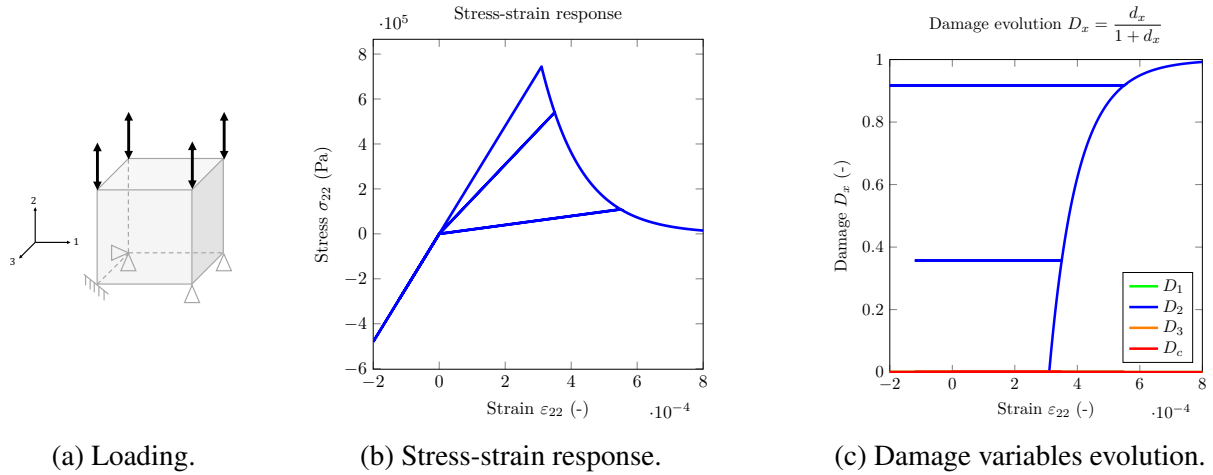


Figure 5: Results for the unidirectional tensile-compression test along direction 2.

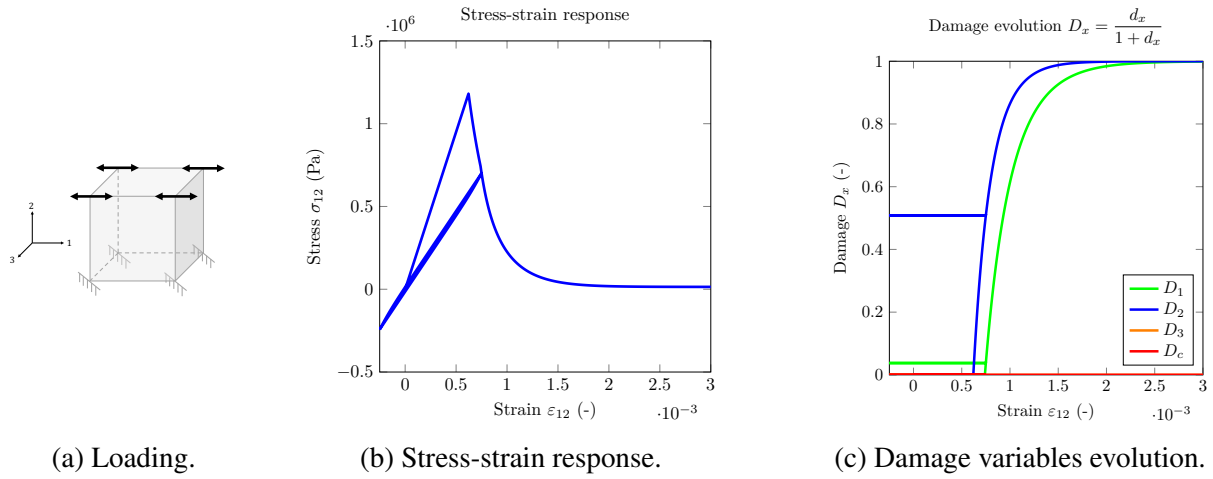


Figure 6: Results for the cyclic shear test along direction 12 without confinement.

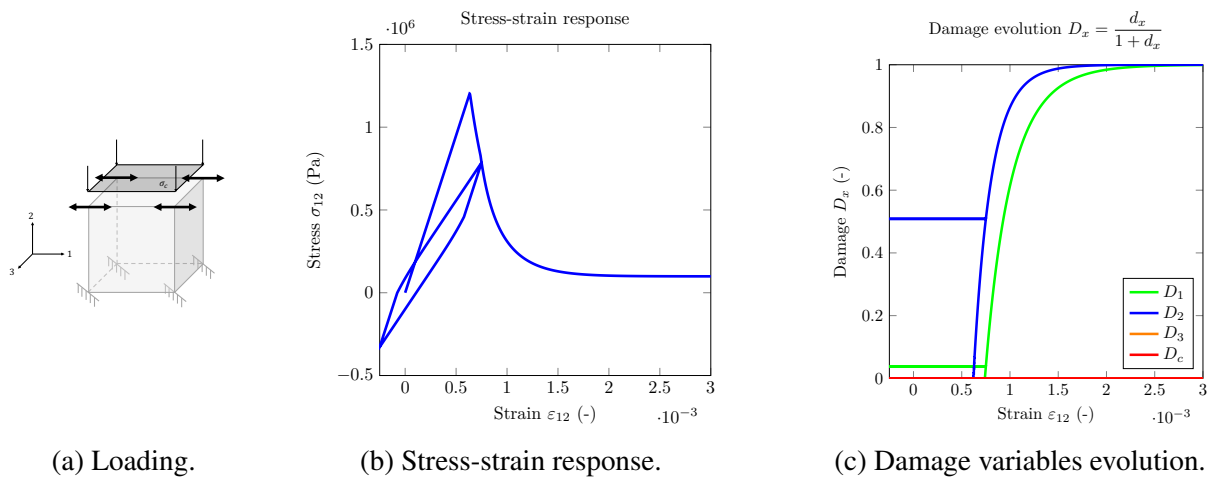


Figure 7: Results for the cyclic shear test along direction 12 with a pre-compression of 0.2MPa.

3.2 Cyclic shear test on a panel (energetic regularisation)

The model is used to perform non-linear static analyses on in-plane loaded masonry walls by studying their overall load-displacement response, the distribution of damage and the energy dissipated. All the numerical results presented in this section were obtained using the Cast3M finite element solver [http://www-cast3m.cea.fr] in which the model was implemented.

Cyclic tests were carried out and compared with the experimental campaign conducted by [3] to analyse the model’s ability to describe the hysteretic response at the scale of the structure. The wall geometry, loading and boundary conditions are presented in Figure 8a. A uniform vertical pre-compression p of 0.6MPa is applied and then held constant while the cyclic horizontal displacement d is applied. Parameter identification was performed upstream on a monotonic shear test representing the envelope curve of the cyclic test.

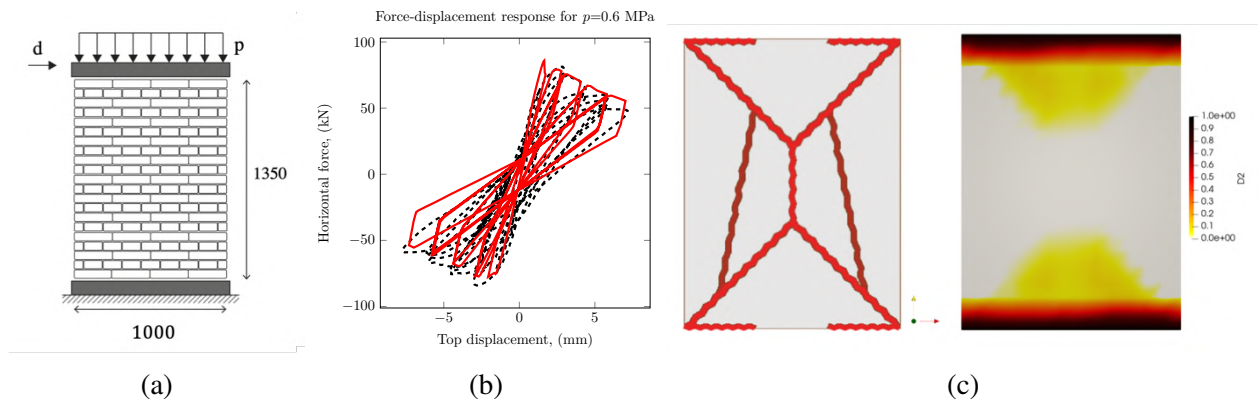


Figure 8: (a) Wall geometry (b) Global $F - u$ response for CUB8 elements of size 0.125m (c) Experimental cracking pattern and numerical damage map [21].

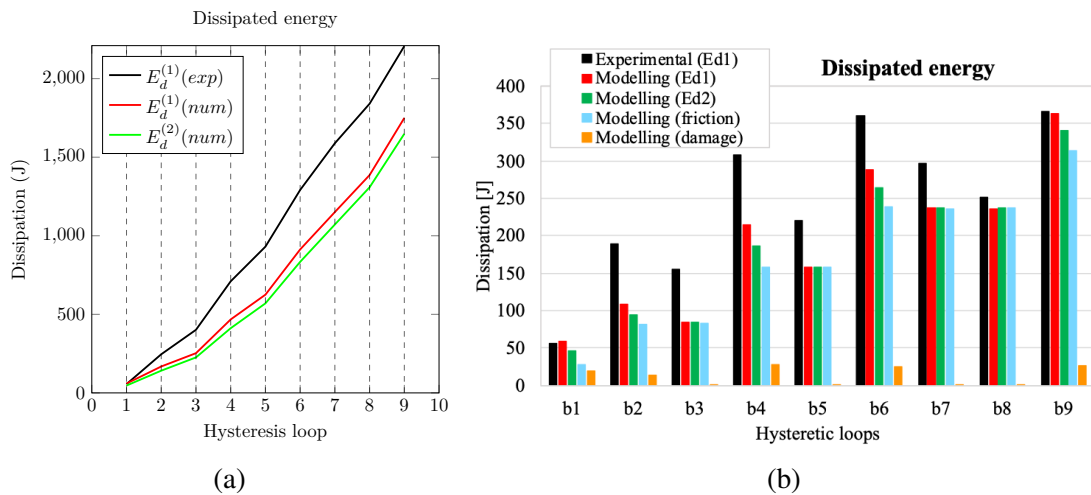


Figure 9: (a) Comparison of the evolution of total experimental and numerical dissipations (b) Energy dissipated per loop and mechanism.

A comparison of the cyclic responses obtained numerically and experimentally suggests a good representation of the overall behaviour of the wall (Fig. 8b). The hysteresis phenomenon develops with the material's progressive degradation: the size of the loops increases with the development of damage (expanded sliding surfaces with the appearance of new cracks). The shear modulus deteriorates with loading. The classic cross-shape characteristic of shear damage is obtained (Fig. 8c).

The general trend in the evolution of dissipation per loop is well represented (Fig. 9a) but the numerical values are lower (except for loops 1, 8 and 9) (Fig. 9b). Under monotonic loading, the main degradation mechanism is damage: cracks tend to open in one direction, so friction is limited. In the case of cyclic loading, friction becomes the main dissipative mechanism. Since \dot{D}_{damage} (Eq. (7)) depends on the damage increment \dot{d}_i , it remains zero if the strain reached in the previous cycle is not exceeded because the damage is not evolving (case of loops 4 and 5) (Fig. 9b). The frictional dissipation $\dot{D}_{sliding}$ stays the same when the cycle is performed several times (case of loops 4 and 5). This leads to a stabilisation of the total dissipation \dot{D} per loop which is found both experimentally and numerically.

3.3 Effect of the regularisation method for a wall under monotonic loading

The choice of regularisation method mainly affects the representation of local quantities such as damage and mesh independence. A wall with a window (Fig. 10) is studied here from a purely numerical point of view to compare the impact of the regularisation techniques.

When no regularisation method is applied (Fig. 11a), the results do not converge to a solution when the mesh is refined. As the dissipated energy is related to the area under the stress-displacement curve (Eq. (8)), it tends towards zero as the mesh size decreases, which is nonphysical. Energetic regularisation requires the mesh size to be reduced (Fig. 11b), whereas non-local regularisation allows the results to

converge more quickly (Fig. 11c). The curves are not exactly the same between the two methods since the brittleness parameter has not been recalibrated.

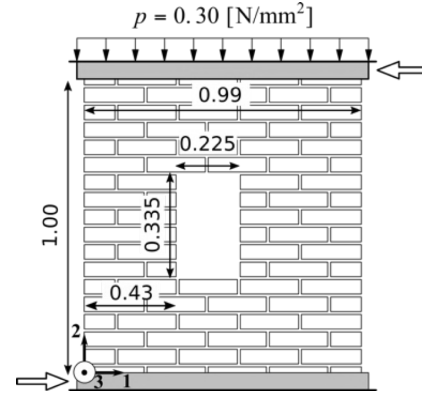


Figure 10: Wall geometry [22].

As far as damage is concerned, the non-local regularisation provides a more diffuse result since the energy dissipation is no longer reduced to a single element, which avoids localising the damage in a line of elements. Even for a coarse mesh size (8cm), the damage map is satisfactory for non-local damage (damage around the window and at the ends of the walls) [22]. Although more costly (Tab. 1), the better mesh convergence of non-local calculations justifies their use.

The dissipations are shown in Figure 13 for the different methods used. It can be seen that when no regularisation technique is used, the dissipation decreases with mesh refinement and the results do not stabilise. For the Hillerborg technique [7], convergence is observed when the mesh size decreases. For the non-local method, total dissipation is almost constant, which can be explained by the convergence speed of the mesh. As expected, the main dissipation mechanism is damage because the loading is monotonic (Fig. 13c versus Fig. 13b).

4 CONCLUSIONS AND PERSPECTIVES

The model's ability to describe the response of masonry to complex loading was illustrated by local tests. In particular, it was able to reproduce the hysteretic loops observed for cyclic

shear loading, as well as the effect of confinement on friction. Numerical analyses on structural elements have shown that the model is capable of satisfactorily representing the overall behaviour of the material (in particular the force-displacement curves). Local quantities, such as the damage field, are qualitatively well reproduced, but a non-local regularisation gives better results. The contributions of dissipa-

tion by degradation mechanism have been estimated. Damage is the main dissipative mechanism for monotonic loading. However, friction takes over as soon as a cyclic behaviour or a discharge phase is initiated. This work provides a first step towards a future assessment of the seismic vulnerability of masonry structures for weak to moderate earthquakes.

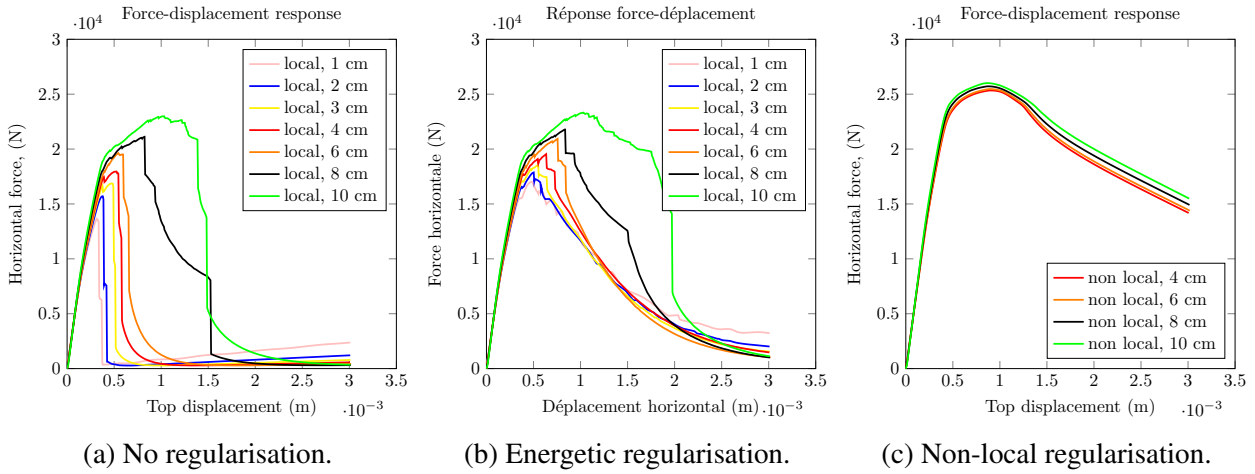


Figure 11: Force-displacement curve for different regularisation methods.

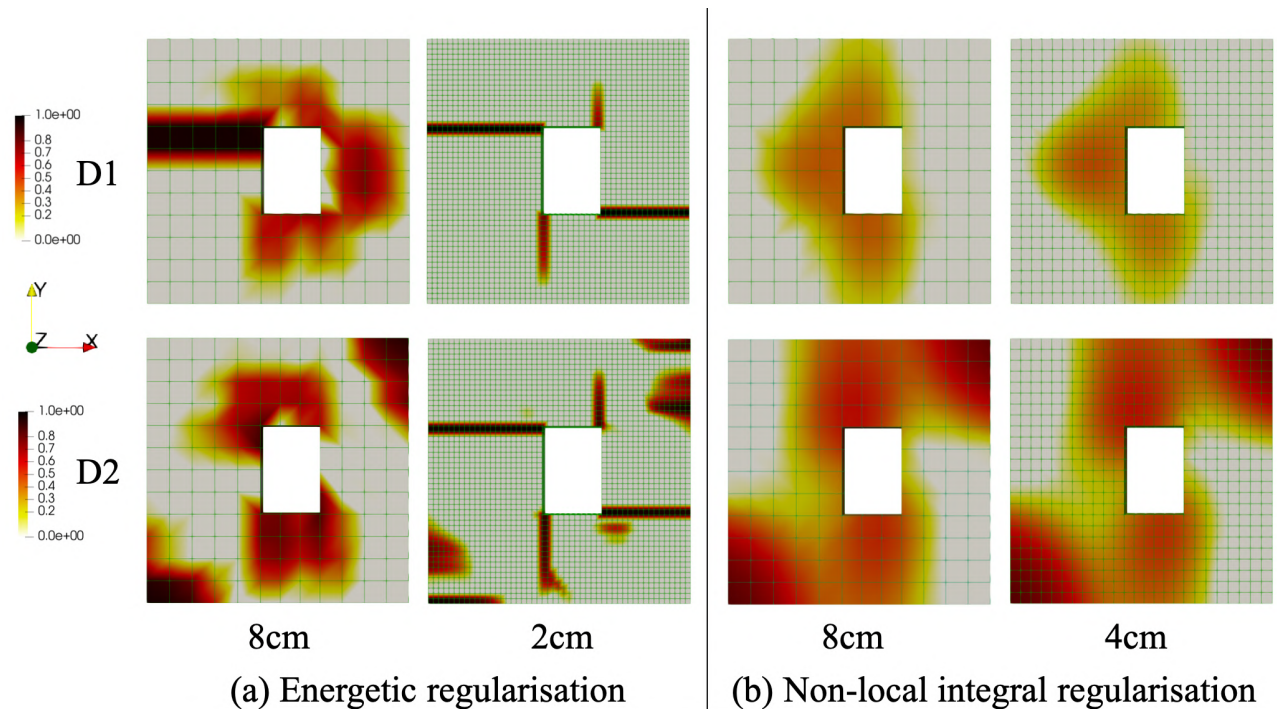


Figure 12: Damage map for different mesh sizes.

Table 1: Calculation time as a function of mesh size and regularisation method.

Techniques	Energetic			Non-local		
Mesh size	8cm	4cm	2cm	8cm	4cm	2cm
Calculation time	2min	13min	2h	5min	3h34	14 days

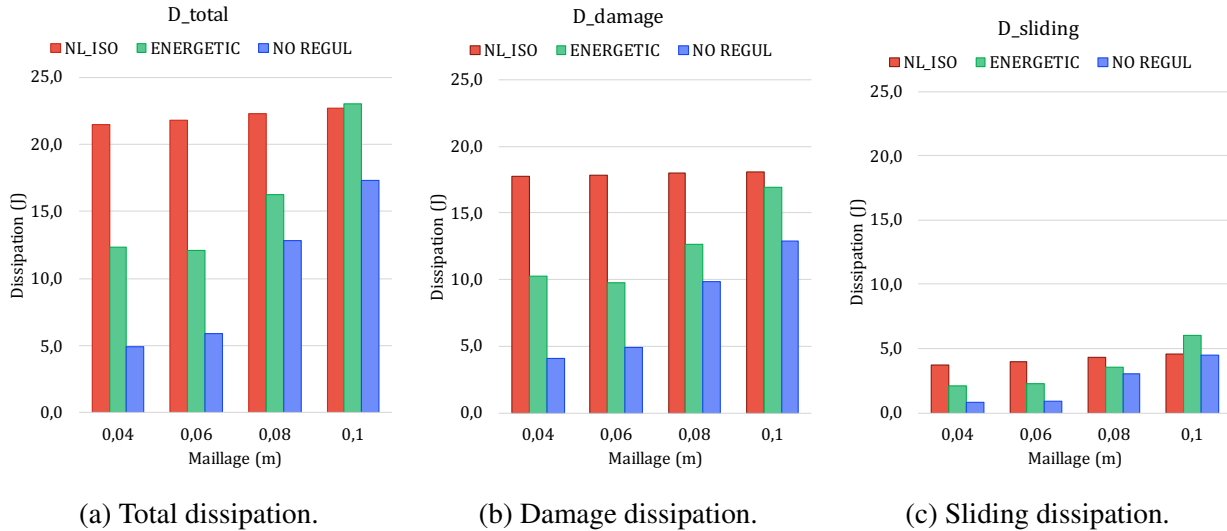


Figure 13: Dissipations for different regularisation techniques and mesh sizes.

REFERENCES

- [1] Addessi, D., Marfia, S., Sacco, E., and Toti J.(2014). Modeling approaches for masonry structures. *The Open Civil Engineering Journal* 8, 288–300.
- [2] Allix, O. and Deü, J.F. (1997). Delay-damage modelling for fracture prediction of laminated composites under dynamic loading. *Engineering Transactions*, 45(1), pp. 29–46.
- [3] Anthoine, A., G. Magonette and G. Magenes (1995). Shear-compression testing and analysis of brick masonry walls. *Tenth European Conference on Earthquake Engineering*, 3, 1657–1662.
- [4] Bourdin, B., Francfort, G.A. and Marigo, J-J. (2000). Numerical experiments in revisited brittle fracture. *Journal of the Mechanics and Physics of Solids* 48.4, pp. 797–826
- [5] Dais, D., I. E. Bal, E. Smyrou and V. Sarhosis. (2021). Automatic crack classification and segmentation on masonry surfaces using convolutional neural networks and transfer learning. *Automation in Construction*, 125, 103606.
- [6] Hillerborg, A., Modeer, M., and Petersson, P. (1976). Analysis of crack formation and crack growth in concrete by means of fracture mechanics and finite elements. *Cement and Concrete Research*, 6(6), 773–781.
- [7] Hillerborg, A. (1978). A model for fracture analysis. *Report TVBM*, 3005. Division of Building Materials, LTH, Lund University.
- [8] Jiràsek, M. and Grassl, P. (2008). Evaluation of directional mesh bias in concrete fracture simulations using continuum damage models. *Engineering Fracture Mechanics*, 75, p. 1921-1943.

- [9] Kachanov, M. (1993). Elastic solids with many cracks and related problems. *Advances in Applied Mechanics*, 30, 259–44.
- [10] Lemaitre, J., Chaboche, J., Benallal, A. and Desmorat, R. (2009). *Mécanique des matériaux solides - 3ème édition*. Dunod.
- [11] Lagomarsino, S., Penna, A., Galasco, A. and Cattari S. (2013). TREMURI program: An equivalent frame model for the non-linear seismic analysis of masonry buildings. *Engineering Structures* 56, 1787–1799.
- [12] Lourenço, P. B. (1996). Computational Strategy for Masonry Structures.
- [13] Marcin, L., J.-F. Maire, N. Carrère and E. Martin (2011). Development of a macroscopic damage model for woven ceramic matrix composites. *International Journal of Damage Mechanics*, 20(6), 939–957.
- [14] Moës, N., Stolz, C., Bernard, P.-E. and Chevaugeon, N. (2011). A level set based model for damage growth: The thick level set approach. *International Journal for Numerical Methods in Engineering*, 86.3, pp. 358–380.
- [15] Moës, N. and Chevaugeon, N. (2021). Lipschitz regularization for softening material models: the Lip-field approach. *Comptes Rendus de Mécanique* 349.2, pp. 415–434
- [16] Peerlings, R. H. J., De Borst, R., Brekelmans, W. A. M. and De Vree, J. H. P. (1996). Gradient enhanced damage for quasi-brittle materials. *International Journal for Numerical Methods in Engineering*, 39, p.3391–3403.
- [17] Pijaudier-Cabot, G. and Bažant, Z. P. (1987). Nonlocal Damage Theory. *Journal of Engineering Mechanics*, 113, p. 1512-1533.
- [18] Roca, P., M. Cervera, G. Gariup and L. Pelà (2010). Structural analysis of masonry historical constructions. classical and advanced approaches. *Archives of Computational Methods in Engineering*, 17, 299–325.
- [19] Sacco, E., D. Addessi, and K. Sab (2018). New trends in mechanics of masonry. *Meccanica*, 53(7), 1565– 1569.
- [20] Sellier, A., G. Casaux-Ginestet, L. Buffo-Lacarrière and X. Bourbon. (2013). Orthotropic damage coupled with localized crack reclosure processing. Part I: Constitutive laws. *Engineering Fracture Mechanics*, 97, 148-167.
- [21] Tisserand, P.-J. , H. Rostagni, C. Giry, T.-T.-H. Nguyen, R. Desmorat and F. Ragueneau. (2022). An orthotropic damage model with internal sliding and friction for masonry-like material. *Engineering Fracture Mechanics*, 267, 108397.
- [22] Vermeltfoort, A., T. Raijmakers and H. Janssen. (1993). Shear tests on masonry walls. In A. Hamid and H. Harris, editors, *6th North American Masonry Conference*, 1183–1193.
- [23] Zeng, B. and Li, Y. (2023) Towards Performance-Based Design of Masonry Buildings: Literature Review. *Buildings*, 13(6), 1534.